Robust Transmit Beamforming for SWIPT-Enabled Cooperative NOMA With Channel Uncertainties

Binbin Su, *Student Member, IEEE*, Qiang Ni, *Senior Member, IEEE*, and Wenjuan Yu, *Member, IEEE*

***Abstract*— In this paper, we study the robust beamforming design for a simultaneous wireless information and power transfer (SWIPT) enabled system, with cooperative non-orthogonal multiple access (NOMA) protocol applied. A novel cooperative NOMA scheme is proposed, where the strong user with better channel conditions adopts power splitting (PS) scheme and acts as an energy-harvesting relay to transmit information to the weak user. The presence of channel uncertainties is considered and incorporated in our formulations to improve the design robustness and communication reliability. Specifically, only imperfect channel state information is assumed to be available at the base station (BS), due to the reason that the BS is far away from both users and suffers serious feedback delay. To comprehensively address the channel uncertainties, two major design criteria are adopted, which are the outage-based constraint design and the worst-case-based optimization. Then, our aim is to maximize the strong user's data rate, by optimally designing the robust transmit beamforming and PS ratio, while guaranteeing the correct decoding of the weak user. With two different channel uncertainty models respectively incorporated, the proposed formulations yield to challenging nonconvex optimization problems. For the outage-based constrained optimization, we first conservatively approximate the probabilistic constraints with the Bernstein-type inequalities, which are then globally solved by 2-D exhaustive search. To further reduce the complexity, an efficient low-complexity algorithm is then proposed with the aid of successive convex approximation (SCA). For the worst-case-based scenario, we first apply the semidefinite relaxation method to relax the quadratic terms and prove the rank-one optimality. Then the nonconvex max-min optimization problem is readily transformed into convex approximations based on *S*-procedure and SCA. Simulation results show that for both channel uncertainty models, the proposed algorithms can converge within a few iterations, and the proposed SWIPT-enabled robust cooperative NOMA system achieves better system performance than the existing protocols.**

***Index Terms*— Non-orthogonal multiple access, simultaneous wireless information and power transfer (SWIPT), outage-based constrained optimization, worst-case-based optimization.**

Manuscript received September 14, 2018; revised January 15, 2019; accepted February 10, 2019. Date of publication February 19, 2019; date of current version June 14, 2019. This work was supported in part by the Royal Society project IEC170324. The associate editor coordinating the review of this paper and approving it for publication was H. Zhang. *(Corresponding author: Qiang Ni.)*

B. Su and Q. Ni are with the School of Computing and Communications, Lancaster University, Lancaster LA1 4WA, U.K. (e-mail: b.su@lancaster.ac.uk; q.ni@lancaster.ac.uk).

W. Yu is with the Institute for Communication Systems, University of Surrey, Guildford GU2 7XH, U.K. (e-mail: w.yu@surrey.ac.uk).

Color versions of one or more of the figures in this paper are available online at http://ieeexplore.ieee.org.

Digital Object Identifier 10.1109/TCOMM.2019.2900318

I. Introduction

NON-ORTHOGONAL multiple access (NOMA) has been proposed as a promising multiple access candidate for 5G and beyond wireless communication systems due to its potential to significantly improve spectral efficiency [1]–[3]. Specifically, NOMA has been shown to be more beneficial than conventional orthogonal multiple access (OMA) schemes in many aspects [4], [5]. For example, in a downlink NOMA network, the base station (BS) sends the superimposed information containing all users' messages, then the users with strong channel conditions can obtain the prior information of the weak users,[1] after applying successive interference cancellation (SIC) to remove the co-channel interference. The obtained prior information can then be fully exploited with a cooperative transmission scheme, to improve the weak user's reception reliability [6].

In addition, since energy efficiency is another key objective of 5G and beyond communications [7], simultaneous wireless information and power transfer (SWIPT) has drawn significant attention [8]. Specifically, the application of SWIPT to NOMA has been studied by considering that NOMA users can harvest energy from the received signals [9]. For instance, the optimal time switching and power splitting (PS) schemes were studied to maximize the achievable rate regions of the wireless powered NOMA systems in [10]. The spectral efficiency performance comparison between NOMA and OMA for a two-user SWIPT system has been addressed in [11]. The cooperative SWIPT NOMA protocol was investigated in [12], in which near NOMA users act as energy harvesting (EH) relays to help far NOMA users without draining their batteries. In [13], considering a cooperative multiple-input single-output (MISO) SWIPT NOMA scheme, the PS ratio and the beamforming vectors were optimized to maximize the data rate of the strong user[2] while satisfying the quality of service (QoS) requirement of the weak user. However, all the above studies assume that perfect channel state information (CSI) is known at the BS, which is quite difficult in practice due to channel estimation errors, feedback delay and quantization errors [14], [15].

By considering a more practical scenario that the BS only knows imperfect CSI, a robust beamforming design problem for MISO NOMA systems was investigated in [16] to maximize the achievable sum rate subject to the transmit power constraint. In [17], the beamformers were designed for

[1]Here, the weak user means the user that is far from the BS.

[2]Here, the strong user means the user that is near the BS.

a robust power minimization problem by incorporating the norm-bounded channel uncertainties to satisfy the required QoS at each user. In addition, to tackle the energy efficiency maximization problem, the robust beamforming design was solved in [18] for a massive multiple-input multiple-output (MIMO) NOMA downlink system with imperfect CSI considered. Furthermore, focusing on a full-duplex MISO MC-NOMA network, a resource allocation algorithm was designed in [19] to maximize the weighted system throughput taking into account the imperfect CSI of the eavesdropping channels and the QoS requirements of legitimate users.

Although channel uncertainties are taken into consideration in the aforementioned papers, we note that SWIPT, as a key enabler of 5G communications [20], is not studied in [16]–[19]. On the other hand, the SWIPT-enabled NOMA in [9]–[13] only considers perfect CSI. Hence, it is natural and of great significance to investigate the transmit beamforming design in a downlink SWIPT-enabled cooperative NOMA system with imperfect CSI. To address the CSI errors, various channel uncertainty models can be found in existing literature. A common one is the outage-based constrained formulation [21] where the outage probability of the signal to interference plus noise ratio (SINR) must be less than a given value. The other is the worst-case SINR constrained problem [22], [23], in which the CSI errors are assumed to lie in a bounded uncertainty set. In this paper, we study both of the channel uncertainty models, in order to provide a comprehensive robust transmit beamforming design. Since in wireless communication systems, the downlink channel can be observed at the receiver side and fed back to the BS via an uplink control channel. Therefore, the main sources which cause imperfect CSI include channel estimation errors *and/or* feedback delay. Specifically, the common pilot with high transmit power is adopted in the downlink channel and shared by all receivers [24]. As a result, there is no channel estimation errors and the CSI obtained at the receiver side can be accurate. Hence we assume that all users perfectly know the CSI of downlink channels in this paper. Despite channel estimations at the user side are accurate, imperfect CSI may still result from feedback delay in the feedback link. As the users are far from the BS, the BS suffers serious feedback delay, which results in imperfect CSI at the BS side. On the other hand, since the two users are quite close to each other, we can assume that the feedback delay at the strong user, i.e., user 1, is negligible. Therefore, user 1 can obtain perfect CSI of user 2, while imperfect CSI is available at the BS. We aim to design robust transmit beamforming to maximize the rate of the strong user, based on the condition that the signal of the weak user can be correctly decoded. The main contributions of this paper are listed in the following:

- To comprehensively study the channel uncertainties for the SWIPT-enabled cooperative NOMA system with only imperfect CSI available at the BS, we formulate new optimization problems to design robust transmit beamforming and PS ratio to maximize the data rate of the strong user by modeling the channel uncertainties as an outage-based SINR constraint and a worst-case SINR constraint, respectively.
- For the robust design of the outage-based constrained formulation P1, we investigate the probabilistic QoS constraints where the probability of failure decoding for the weaker user's signal must fall below a given outage value. Semidefinite relaxation (SDR) technique is firstly employed to linearize the quadratic terms in the SINR expression. Then we derive an efficiently computable convex approximation of the original problem with the Bernstein-type inequality method, which can be globally solved. To avoid the high complexity, the successive convex approximation (SCA)-based method is then proposed to iteratively solve the problem. We verify that the proposed Bernstain-inequality and SCA-based transformation method can *usually* produce the rank-one solutions.
- For the worst-case-based formulation P4, the SDR method is first applied and the rank-one optimality of the SDR approach is demonstrated to show the equivalence with the original problem. Then the reformulated robust design using *S*-procedure is presented to solve the hidden inner minimization constraint over the norm-bounded error. Finally, an efficient iterative algorithm based on SCA is developed to provide a low-complexity robust beamforming design.
- Simulation results demonstrate the robustness and effectiveness of the proposed beamforming design compared to other existing schemes for both rate-maximization formulations and channel uncertainty models. In addition, it shows that both the proposed low-complexity algorithms can achieve near-optimal system performance.

The rest of this paper is organized as follows. In Section II, we give a brief introduction to the system model of the proposed SWIPT-enabled robust cooperative NOMA system. The probabilistic SINR constrained optimization problem is formulated and analyzed in Section III. In Section IV, the data rate maximization problem for the strong user is formulated and solved by adopting the worst-case-based channel uncertainty model. Simulation results are given in Section V and finally the paper is concluded in Section VI.

The following notation is used: $\mathbb{E}\{\cdot\}$ represents expectation, $(\cdot)^T$ denotes the Hermitian transpose, $\text{Tr}(\cdot)$ and $\text{rank}(\cdot)$ means the trace and the rank of a matrix, and $\mathbf{I}$ is an identity matrix of appropriate dimension. $|\cdot|$ denotes the absolute value of a complex scalar, $||\cdot||$ denotes the l_2 norm of a vector. The circularly symmetric complex Gaussian distribution with mean μ and variance σ^2 is denoted by $\mathcal{CN}(\mu, \sigma^2)$.

II. System Model

Consider a downlink time division multiple access (TDMA) MISO transmission system, as shown in Fig. 1, wherein the BS is equipped with N_t antennas and all users are equipped with the single antenna. There are two users in each beam and the BS performs MISO transmission with K users through M beams, where $K = 2M$.[3] Assume that the total time duration T is equally divided into M slots where the time duration of

[3]It is assumed that users have already been grouped into pairs, and we can refer to [25] for how to do user pairing.

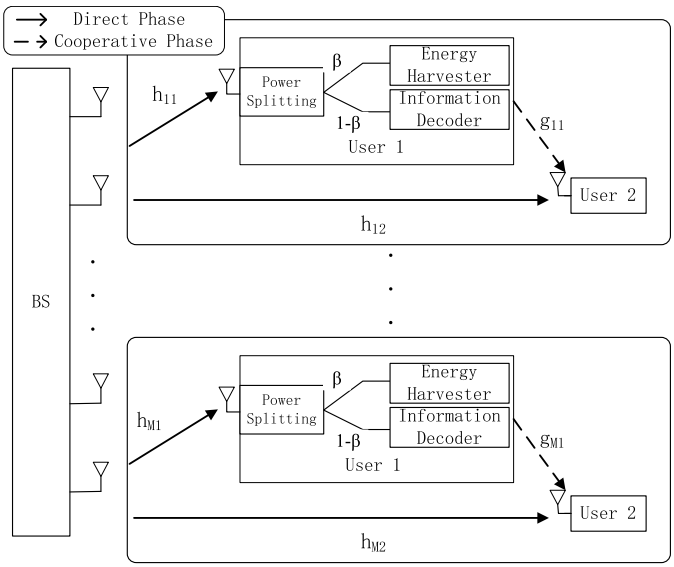

Fig. 1. System model for the SWIPT-enabled cooperative NOMA.

each slot is $t_m = \frac{T}{M}$. Then during the time slot t_m, only the m-th user-pair is allowed to transmit, while the other user-pairs remain silent. Therefore, the inner-cell interference between pairs of users does not exist. As a result, when formulating the rate-maximization problems and designing robust beamforming, we can just focus on one beam.

Let us take the first beam as an example. It is assumed that NOMA protocol is adopted for the two users. Without loss of generality, we assume that user 1 is a strong user with better channel conditions and user 2 is a weak user. According to NOMA protocol, user 1 removes the interference of user 2 by applying SIC and then detect its own information, while the user 2 treats the user 1's message as noise. Since user 1 can obtain prior information of the messages for user 2 and thus can act as a relay to improve the connection between the BS and user 2. In order to help user 2 without draining user 1's battery, we assume that the power utilized to transmit the information of user 2 can be obtained from SWIPT.

Since the imperfect CSI case at the BS is considered, we first introduce the CSI error model. The actual channels between the BS and two users can be characterized as

$$\boldsymbol{h}_i = \tilde{\boldsymbol{h}}_i + \boldsymbol{e_i}, \quad i = 1, 2, \tag{1}$$

where $\boldsymbol{h}_i$ denotes the actual channel gain, $\tilde{\boldsymbol{h}}_i$ is the estimated channel gain at the BS, and $\boldsymbol{e_i}$ represents the channel errors of two users. The detailed expression of $\boldsymbol{e_i}$ for the two channel uncertainty models will be introduced in the next two sections.

Two phases are involved in the SWIPT-enabled robust cooperative NOMA transmission. At the first *robust direct transmission phase*, user 1 coordinates the process of information decoding (ID) and EH from the received signal by adopting PS scheme. Specifically, as can be seen in Fig. 1, the received signal at user 1 is split into the information decoder and the energy harvester. As for user 2, it receives the direct transmission signal from the BS at this phase. Then in the second *cooperative transmission phase*, user 1 forwards the decoded user 2's message to user 2 with the harvested energy. The detailed process is summarized as follows.

A. Robust Direct Transmission Phase

During this phase, the signals for two users are superposition coded at the BS, i.e., $\boldsymbol{x} = \boldsymbol{w}_1 x_1 + \boldsymbol{w}_2 x_2$, where x_1 and x_2 are the messages for user 1 and user 2 respectively. The power of the transmitted symbol is normalized, i.e., $\mathbb{E}\|x_1\|^2 = \mathbb{E}\|x_2\|^2 = 1$, and $\boldsymbol{w}_1$ and $\boldsymbol{w}_2$ are the corresponding precoding vector. Then, for the weak user, i.e., user 2, the observation is given by

$$y_2^{(1)} = \boldsymbol{h}_2^H(\boldsymbol{w}_1 x_1 + \boldsymbol{w}_2 x_2) + n_2, \tag{2}$$

where $\boldsymbol{h}_2^H$ denotes the Hermitian transpose of $\boldsymbol{h}_2 \in \mathbb{C}^{Nt}$, $n_2 \sim \mathcal{CN}(0,1)$ is the additive white Gaussian noise (AWGN). In this paper, we assume that all channels have the same noise value as $\sigma^2 = 1$. Then the SINR obtained by user 2 from the direct transmission can be expressed as

$$\mathrm{SINR}_2^{(1)} = \frac{|\boldsymbol{h}_2^H \boldsymbol{w}_2|^2}{1 + |\boldsymbol{h}_2^H \boldsymbol{w}_1|^2}. \tag{3}$$

Due to the assumption that there is not enough power to forward the signal of x_2 to user 2, user 1 needs to replenish the energy from the BS based on the 'harvest-then-transmit' protocol proposed in [26]. The PS scheme is employed at user 1 to perform SWIPT. Then, the information received at user 1 is given by

$$y_1 = \sqrt{1-\beta}\boldsymbol{h}_1^H(\boldsymbol{w}_1 x_1 + \boldsymbol{w}_2 x_2) + n_1, \tag{4}$$

where $\beta \in [0,1]$ is the PS ratio, $\boldsymbol{h}_1 \in \mathbb{C}^{Nt}$ is the channel coefficient between the BS and user 1, and $n_1 \sim \mathcal{CN}(0,1)$ is the AWGN. With SIC carried out at user 1, i.e., user 1 firstly decodes the message for user 2 and then removes the information of user 2 to decode its own information, the received SINR for user 1 to detect the message of user 2, is given by

$$\mathrm{SINR}_{1,2} = \frac{(1-\beta)|\boldsymbol{h}_1^H \boldsymbol{w}_2|^2}{1 + (1-\beta)|\boldsymbol{h}_1^H \boldsymbol{w}_1|^2}. \tag{5}$$

After removing the message of user 2 from y_1, the corresponding signal to noise ratio (SNR) of user 1 can be expressed as

$$\mathrm{SNR}_1 = (1-\beta)|\boldsymbol{h}_1^H \boldsymbol{w}_1|^2, \tag{6}$$

which will be our optimization objective in the next section.

Besides, to ensure the correct decoding capability in a given order, we have the following inequality requirements [27]:

$$|\boldsymbol{h}_1^H \boldsymbol{w}_2|^2 \geq |\boldsymbol{h}_1^H \boldsymbol{w}_1|^2, \tag{7a}$$

$$|\boldsymbol{h}_2^H \boldsymbol{w}_2|^2 \geq |\boldsymbol{h}_2^H \boldsymbol{w}_1|^2. \tag{7b}$$

Furthermore, with PS protocol applied at user 1 to harvest energy from the BS, the harvested energy can be given as [28]

$$E = \zeta\beta(|\boldsymbol{h}_1^H \boldsymbol{w}_1|^2 + |\boldsymbol{h}_1^H \boldsymbol{w}_2|^2)\mathrm{T}, \tag{8}$$

where ζ and T denote the EH efficiency and the transmission time fraction, respectively. Without loss of generality, we set

$\mathrm{T} = \frac{1}{2}$ which means that equal time duration is assigned for direct and cooperative transmission stages. Hence, the available average power of user 1 can be expressed as

$$P_r = \frac{\zeta\beta(|\boldsymbol{h}_1^H\boldsymbol{w}_1|^2 + |\boldsymbol{h}_1^H\boldsymbol{w}_2|^2)T}{1-T} = \zeta\beta(|\boldsymbol{h}_1^H\boldsymbol{w}_1|^2 + |\boldsymbol{h}_1^H\boldsymbol{w}_2|^2). \quad (9)$$

It is worthwhile to point out that only when user 1 can successfully decode the signals of two users, it can then use the harvested energy to forward the signals to user 2. This means that it is more important for user 1 to decode the signals than performing EH.

B. Cooperative Transmission Phase

In the cooperative transmission phase, if the received SINR for user 1 to detect the message of user 2 is larger than or equal to the target SINR of user 2, we can assume that user 1 can correctly decode the received symbols of user 2 [29]. Then user 1 forwards signal x_2 to user 2 using the harvested energy. The observation of user 2 at this phase can be characterized as

$$y_2^{(2)} = \sqrt{P_r}gx_2 + n_3, \quad (10)$$

where P_r is the available power of user 1, g is the perfectly known channel coefficient between user 1 and user 2, and $n_3 \sim \mathcal{CN}(0,1)$ is the normalized AWGN. The achievable SNR of user 2 at this phase can be written as

$$\mathrm{SNR}_2^{(2)} = \zeta\beta|g|^2(|\boldsymbol{h}_1^H\boldsymbol{w}_1|^2 + |\boldsymbol{h}_1^H\boldsymbol{w}_2|^2). \quad (11)$$

Combining the observation from both phases and using maximal ratio combination (MRC), the equivalent SINR of user 2 can be finally obtained as

$$\mathrm{SINR}_2 = \mathrm{SINR}_2^{(1)} + \mathrm{SNR}_2^{(2)} = \frac{|\boldsymbol{h}_2^H\boldsymbol{w}_2|^2}{1+|\boldsymbol{h}_2^H\boldsymbol{w}_1|^2} + \zeta\beta|g|^2(|\boldsymbol{h}_1^H\boldsymbol{w}_1|^2 + |\boldsymbol{h}_1^H\boldsymbol{w}_2|^2). \quad (12)$$

In the next two sections, we aim to maximize the data rate of user 1, which is equivalent to maximize the SNR of user 1, subject to the outage-based and worst-case-based constraints respectively.

III. Outage-Based Constrained Optimization

In this section, the outage-based probabilistic constraints caused by imperfect CSI will be investigated, where the unsuccessful decoding of weak user falls into the scope of outage. The goal is to design beamforming vectors $\boldsymbol{w}_1$ and $\boldsymbol{w}_2$ to maximize the data rate of user 1, which is equivalent to maximize the SNR of user 1 while guaranteeing the outage requirements. Specifically, the outage for strong user happens when it is not able to decode the weaker user's information, while for the weak user, the outage means that it cannot successfully decode its own information.

The study of outage-based constrained robust optimization is a meaningful design criterion as CSI errors are universal present in practical systems, and they may cause severe outage if not handled properly [30]. However, as the probability functions cannot yield straightforward closed-form expressions, how to deal with probabilistic constraints is of vital importance. To tackle the problem, we will resort to Bernstein-type inequality approach to deal with the probability constraints.

We consider the following robust beamforming design problem:

$$\begin{aligned}
\mathrm{P1}: \max_{\beta,\boldsymbol{w}_1,\boldsymbol{w}_2} \ & (1-\beta)|\boldsymbol{h}_1^H\boldsymbol{w}_1|^2 && (13a)\\
\text{s.t. } & \Pr\left(\mathrm{SINR}_{1,2} \geq \gamma\right) \geq 1-\rho_1, && (13b)\\
& \Pr\left(\mathrm{SINR}_2 \geq \gamma\right) \geq 1-\rho_2, && (13c)\\
& ||\boldsymbol{w_1}||_2^2 + ||\boldsymbol{w_2}||_2^2 \leq P_{max}, && (13d)\\
& |\boldsymbol{h}_1^H\boldsymbol{w}_2|^2 \geq |\boldsymbol{h}_1^H\boldsymbol{w}_1|^2, && (13e)\\
& |\boldsymbol{h}_2^H\boldsymbol{w}_2|^2 \geq |\boldsymbol{h}_2^H\boldsymbol{w}_1|^2, && (13f)\\
& 0 \leq \beta \leq 1, && (13g)
\end{aligned}$$

where γ is the target SINR of user 2, $\rho_i \in [0,1)$, $i = 1,2$, is the maximum tolerable outage probability for two users, and P_{max} is the maximum available power at the BS. Constraints (13e) and (13f) represent the given order decoding capability requirements [27].

To solve the problem P1, we first relax it by applying SDR approach and drop the rank-one constraint. Specifically, we replace the beamforming vector $\boldsymbol{w}_i$ by semidefinite positive matrices $\boldsymbol{W}_i$, i.e,

$$\boldsymbol{W}_i = \boldsymbol{w}_i\boldsymbol{w}_i^H, \quad i = 1,2. \quad (14)$$

Then, since imperfect CSI is considered at the BS, the channel errors can be modeled as

$$\boldsymbol{e_i} = \boldsymbol{C}_i^{\frac{1}{2}}\boldsymbol{e}, \quad i = 1,2, \quad (15)$$

where $\boldsymbol{C}_i \succeq \boldsymbol{0}$ denotes some known error covariance and $\boldsymbol{e} \sim \mathcal{CN}(\boldsymbol{0}, \mathbf{I}_{N_t})$.

By replacing $\boldsymbol{h}_i$ with $\tilde{\boldsymbol{h}}_i + \boldsymbol{C}_i^{\frac{1}{2}}\boldsymbol{e}$ and denoting that $\Gamma = (\tilde{\boldsymbol{h}}_1 + \boldsymbol{C}_1^{\frac{1}{2}}\boldsymbol{e})^H(\boldsymbol{W}_2 - \gamma\boldsymbol{W}_1)(\tilde{\boldsymbol{h}}_1 + \boldsymbol{C}_1^{\frac{1}{2}}\boldsymbol{e})$, the probabilistic SINR constraint (13b) can be recast as

$$\Pr\left(\Gamma \geq \frac{\gamma}{1-\beta}\right) \geq 1-\rho_1. \quad (16)$$

On the other hand, for the outage-based SINR constraint (13c), we transform it by introducing an auxiliary variable θ. Firstly, (13c) can be decomposed into the following two sub-problems:

$$\begin{aligned}
& \Pr\left\{\zeta\beta|g|^2(|\boldsymbol{h}_1^H\boldsymbol{w}_1|^2 + |\boldsymbol{h}_1^H\boldsymbol{w}_2|^2) \geq \gamma - \theta\right\} \geq 1-\rho_2, && (17a)\\
& \frac{|\boldsymbol{h}_2^H\boldsymbol{w}_2|^2}{|\boldsymbol{h}_2^H\boldsymbol{w}_1|^2 + 1} \geq \theta, && (17b)
\end{aligned}$$

where the optimality of the decomposition can be assured when (17b) holds with equality. It is worth noting that (17a) has the same form as (13b). Furthermore, with the application of SDR, (17b) can be further described as

$$\theta\mathrm{Tr}(\boldsymbol{H}_2\boldsymbol{W}_1) \leq \mathrm{Tr}(\boldsymbol{H}_2\boldsymbol{W}_2) - \theta, \quad (18)$$

where $\boldsymbol{H}_i \triangleq \boldsymbol{h}_i\boldsymbol{h}_i^H, i = 1,2$.

Further, by introducing several auxiliary variables, i.e., Q_i, r_i and $s_i, i = 1, 2$, the following correspondence to (13b) and (17a) can be shown

$$\boldsymbol{Q}_1 = \boldsymbol{C_1}^{\frac{1}{2}}(\boldsymbol{W}_2 - \gamma \boldsymbol{W}_1)\boldsymbol{C_1}^{\frac{1}{2}}, \tag{19a}$$
$$\boldsymbol{r}_1 = \boldsymbol{C_1}^{\frac{1}{2}}(\boldsymbol{W}_2 - \gamma \boldsymbol{W}_1)\tilde{\boldsymbol{h}}_1, \tag{19b}$$
$$s_1 = \tilde{\boldsymbol{h}}_1^H(\boldsymbol{W}_2 - \gamma \boldsymbol{W}_1)\tilde{\boldsymbol{h}}_1 - \frac{\gamma}{1-\beta}, \tag{19c}$$
$$\boldsymbol{Q}_2 = \boldsymbol{C_1}^{\frac{1}{2}}(\boldsymbol{W}_1 + \boldsymbol{W}_2)\boldsymbol{C_1}^{\frac{1}{2}}, \tag{19d}$$
$$\boldsymbol{r}_2 = \boldsymbol{C_1}^{\frac{1}{2}}(\boldsymbol{W}_1 + \boldsymbol{W}_2)\tilde{\boldsymbol{h}}_1, \tag{19e}$$
$$s_2 = \tilde{\boldsymbol{h}}_1^H(\boldsymbol{W}_1 + \boldsymbol{W}_2)\tilde{\boldsymbol{h}}_1 - \frac{\gamma - \theta}{\zeta\beta|g|^2}. \tag{19f}$$

Finally, the original probabilistic outage constraint (13b) and the reformulated (17a) can be written as the following same structure

$$\Pr\left\{\boldsymbol{e}^H\boldsymbol{Q}_i\boldsymbol{e} + 2Re\{\boldsymbol{e}^H\boldsymbol{r}_i\} + s_i \geq 0\right\} \geq 1 - \rho_i, \quad i = 1, 2. \tag{20}$$

A. Bernstein-Type Inequality Method

To deal with a probabilistic constraint that has a form as (20), we adopt the Bernstein-type inequality to construct a convex approximation. Firstly, the following lemma is introduced which serves as a basis [31]:

Lemma 1: Let $\boldsymbol{e} \in \mathcal{CN}(0, \mathbf{I}_\mathrm{n})$, $\boldsymbol{Q} \in \mathbb{H}^n$ and $\boldsymbol{r} \in \mathbb{C}^n$. Then, for any $\varepsilon > 0$, we have that

$$\Pr\{\boldsymbol{e}^H\boldsymbol{Q}_i\boldsymbol{e} + 2Re\{\boldsymbol{e}^H\boldsymbol{r}_i\} \geq T(\varepsilon)\} \geq 1 - e^{-\varepsilon}, \tag{21}$$

where the function T is defined by that:

$$\mathrm{T}(\varepsilon) = \mathrm{Tr}(\boldsymbol{Q}_i) - \sqrt{2\varepsilon}\sqrt{||\boldsymbol{Q}_i||_F^2 + 2||\boldsymbol{r}_i||^2} - \varepsilon\lambda^+(\boldsymbol{Q}_i), \tag{22}$$

with $\lambda^+(\boldsymbol{Q}_i) = \max\{\lambda_{max}(-\boldsymbol{Q}_i), 0\}$, and λ_{max} denotes the corresponding maximum eigenvalue of $-\boldsymbol{Q}_i$.

The above inequality is the well-known Bernstein-type inequality, which can also be expressed by the inverse mapping T^{-1} as follows due to the monotonically decreasing characteristic of $\mathrm{T}(\varepsilon)$:

$$\Pr\left\{\boldsymbol{e}^H\boldsymbol{Q}_i\boldsymbol{e} + 2\mathrm{Re}\{\boldsymbol{e}^H\boldsymbol{r}_i\} + s_i \geq 0\right\} \geq 1 - e^{-\mathrm{T}^{-1}(-\mathrm{s})}. \tag{23}$$

It is easy to find that when $e^{-T^{-1}(-s_i)} \leq \rho_i$ holds, the inequality (23) can still be satisfied if we replace $e^{-T^{-1}(-s_i)}$ with ρ_i. By adopting the Bernstain-type inequality and using the monotonically decreasing characteristic of T, we can obtain that

$$\mathrm{Tr}(\boldsymbol{Q}_i) + \ln(\rho_i)\lambda^+(\boldsymbol{Q}_i) - s_i\sqrt{-2\ln(\rho_i)}\sqrt{||\boldsymbol{Q}_i||_F^2 + 2||\boldsymbol{r}_i||^2} \geq 0. \tag{24}$$

Furthermore, by introducing two slack variables $t_1 \in \mathbb{R}$ and $t_2 \in \mathbb{R}$, (24) can be reformulated as the following convex conic inequalities:

$$\mathrm{Tr}(\boldsymbol{Q}_i) - \sqrt{-2\ln(\rho_i)}t_1 + \ln(\rho_i)t_2 + s_i \geq 0, \tag{25a}$$
$$\sqrt{||\boldsymbol{Q}||_F^2 + 2||\boldsymbol{r}_i||^2} \leq t_1, \tag{25b}$$
$$t_2\mathbf{I}_n + \boldsymbol{Q}_i \succeq \mathbf{0}, \tag{25c}$$
$$t_2 \geq 0. \tag{25d}$$

Therefore, one can note that the probabilistic inequality (20) is transformed into efficiently computable convex restrictions as (25a)-(25d).

Finally, by applying the SDR approach and Bernstein-type method, P1 is reformulated as

$$\mathrm{P2}: \max_{\beta, \boldsymbol{W}_1, \boldsymbol{W}_2} \ (1-\beta)\mathrm{Tr}(\boldsymbol{H}_1\boldsymbol{W}_1) \tag{26a}$$
$$s.t.\ \mathrm{Tr}(\boldsymbol{Q}_1) - \sqrt{-2\ln(\rho_1)}t_1 + \ln(\rho_1)t_2 + s_1 \geq 0, \tag{26b}$$
$$\sqrt{||\boldsymbol{Q}_1||_F^2 + 2||\boldsymbol{r}_1||^2} \leq t_1, \tag{26c}$$
$$t_2\mathbf{I}_n + \boldsymbol{Q}_1 \succeq \mathbf{0}, \tag{26d}$$
$$\mathrm{Tr}(\boldsymbol{Q}_2) - \sqrt{-2\ln(\rho_2)}t_3 + \ln(\rho_2)t_4 + s_2 \geq 0, \tag{26e}$$
$$\sqrt{||\boldsymbol{Q}_2||_F^2 + 2||\boldsymbol{r}_2||^2} \leq t_3, \tag{26f}$$
$$t_4\mathbf{I}_n + \boldsymbol{Q}_2 \succeq \mathbf{0}, \tag{26g}$$
$$t_2 \geq 0, t_4 \geq 0, \tag{26h}$$
$$\theta\mathrm{Tr}(\boldsymbol{H}_2\boldsymbol{W}_1) \leq \mathrm{Tr}(\boldsymbol{H}_2\boldsymbol{W}_2) - \theta, \tag{26i}$$
$$\mathrm{Tr}(\boldsymbol{H}_1\boldsymbol{W}_2) \geq \mathrm{Tr}(\boldsymbol{H}_1\boldsymbol{W}_1), \tag{26j}$$
$$\mathrm{Tr}(\boldsymbol{H}_2\boldsymbol{W}_2) \geq \mathrm{Tr}(\boldsymbol{H}_2\boldsymbol{W}_1), \tag{26k}$$
$$\mathrm{Tr}(\boldsymbol{W}_1) + \mathrm{Tr}(\boldsymbol{W}_2) \leq P_{max}, \tag{26l}$$
$$0 \leq \beta \leq 1, \tag{26m}$$

where Q_i, r_i and $s_i, i = 1, 2$, are defined as (19a)-(19f).

Remark 1: The optimal solution to problem P2 can be found through two-dimensional (2-D) exhaustive search of variables β and θ.

However, the complexity of 2-D exhaustive search is too high, which motivates us to find a low-complexity suboptimal solution based on SCA and arithmetic geometric mean (AGM) [32].

B. SCA-Based Transformation

In this subsection, before we solve the formulated problem P2, we first transform it into a convex program. By applying epigraph reformulation and introducing two auxiliary variables μ an ν, the objective function (26a) can be recast as:

$$\max \ \mathrm{u} \tag{27a}$$
$$s.t.\ \nu^2 \geq \mu, \tag{27b}$$
$$\begin{bmatrix} 1-\beta & \nu \\ \nu & \mathrm{Tr}(\boldsymbol{H}_1\boldsymbol{W}_1) \end{bmatrix} \succeq 0. \tag{27c}$$

Hence, (26a) is converted into a linear objective function (27a), a convex linear matrix inequality (LMI) (27c) and a nonconvex quadratic inequality (27b) which can be then approximated by the SCA method. To approximate (27b), a convex lower bound for ν^2 needs to be obtained by applying first-order Taylor approximation as below:

$$\nu^2 \geq 2\nu^{(n)}\nu - (\nu^{(n)})^2, \tag{28}$$

where $\nu^{(n)}$ denotes the value of variable ν at the n-th iteration. By replacing ν^2 with the inequality (28), (27b) can be approximated by a stringent constraint given as

$$2\nu^{(n)}\nu - (\nu^{(n)})^2 \geq \mu. \tag{29}$$

Algorithm 1 SCA-Based Method to Solve P3

1: Input: $\mu_0 = 0.001$, $\nu_0 = 0.01$ $n = 0$, $\eta = 1$ and the tolerance $\epsilon = 10^{-3}$.
2: **while** $\eta \geq \epsilon$
3: Update μ^n by solving problem (33);
4: Set $\mu^n = \mu^{n-1}$;
5: Update $\eta = \mu^n - \mu^{n-1}$;
6: Update $n = n + 1$;
7: **end while**
8: Output: $\boldsymbol{W}_1^n$ and $\boldsymbol{W}_2^n$.

In addition, by applying AGM method, the constraint (26i) can be approximated using the following convex function:

$$\left(a_1^{(n)}\theta\right)^2 + \left(\mathrm{Tr}(\boldsymbol{H}_2\boldsymbol{W}_1)/a_1^{(n)}\right)^2 \leq 2\mathrm{Tr}(\boldsymbol{H}_2\boldsymbol{W}_2) - 2\theta, \quad (30)$$

where the setting of $a_1^{(n)}$ can be given by

$$a_1^{(n)} = \sqrt{(\mathrm{Tr}(\boldsymbol{H}_2^H\boldsymbol{W}_1)^{(n-1)}/\theta^{(n-1)}}. \quad (31)$$

Now the remaining problem lies in (26e), as the formation of s_2 is nonconvex. By introducing a slack variable ξ, s_2 can be reformulated as

$$s_2 = \tilde{\boldsymbol{h}}_1^H(\boldsymbol{W}_1 + \boldsymbol{W}_2)\tilde{\boldsymbol{h}}_1 - \frac{\gamma}{\zeta\beta|g|^2} + \xi, \quad (32a)$$

$$\left(a_2^{(n)}\beta\right)^2 + \left(\xi/a_2^{(n)}\right)^2 \leq \frac{2\theta}{\zeta|g|^2}, \quad (32b)$$

where $a_2^{(n)} = \sqrt{\xi^{(n-1)}/\beta^{(n-1)}}$. Here, (32b) is obtained with the AGM-inequality method and the transformation process is omitted for simplicity.

As a result, after applying the proposed approximation methods, the original problem P2 can be transformed to a convex program. During the n-th iteration, the following convex optimization problem needs to be solved:

$$\mathrm{P3}: \max_{\mu,\nu,\beta,\boldsymbol{W}_1,\boldsymbol{W}_2} \ \mu \quad (33a)$$

$$s.t.\ 2\nu^{(n)}\nu - (\nu^{(n)})^2 \geq \mu, \quad (33b)$$

$$\begin{bmatrix} 1-\beta & \nu \\ \nu & \mathrm{Tr}(\boldsymbol{H}_1\boldsymbol{W}_1) \end{bmatrix} \succeq 0, \quad (33c)$$

$$(26b), (26c), (26d), (26e), (26f), (26g), (26h), \quad (33d)$$

$$(26j), (26k), (26l), (27c), (29), (30), (32a), (32b). \quad (33e)$$

Finally, to solve the problem P3, we provide the SCA-based iterative algorithm, outlined in Algorithm 1.

To prove the effectiveness of the proposed Algorithm 1, we provide the following proposition.

Proposition 1: The proposed Algorithm 1 based on the SCA method can converge to a Karush-Kuhn-Tucker (KKT) point of problem P2 whenever problem P3 is feasible.

Proof: The convergence of SCA method will be proved in Proposition 3 in the next section.

It is noted that both problem P2 and P3 are formulated by dropping the rank-one constraint. We verify the rank-one characteristic of problem P3 via simulations by setting $\gamma = 1$ Mbps, and $\rho = 0.1$. The solution is declared as rank-one if the following condition holds:

$$\frac{\lambda_{max}(\boldsymbol{W}_i)}{\mathrm{Tr}(\boldsymbol{W}_i)} = 1, \quad i = 1, 2. \quad (34)$$

We iteratively solve the optimization problems for 1,000 times. As can be seen from Table I, in the ratio column, the denominator represents the number of feasible points while the numerator denotes the amount of rank-one solutions. The probability of rank-one solutions is higher than 98%, which means the rank-one solutions are *usually* obtained. Hence, we can conclude that the solutions of problem P3 guarantee that the rank-one constraints can be satisfied with a high probability, which provides a tight upper bound on the optimal values of the original problem formulation.

TABLE I
RATIO OF RANK-ONE SOLUTIONS

P_{max}	10 dB	20 dB	30 dB
Ratio	$\frac{297}{297}$	$\frac{859}{876}$	$\frac{954}{971}$

IV. WORST-CASE-BASED OPTIMIZATION

Apart from the outage-based channel uncertainty model, in this section the channel uncertainties are modeled based on the worst-case scenario. Firstly, let us discuss the channel mismatches. For worst-case-based optimization, the channel mismatches are assumed to lie in the bounded sets $\{\tilde{\boldsymbol{e}}_{h_1} : ||\tilde{\boldsymbol{e}}_{h_1}||^2 \leq \epsilon_{h_1}^2\}$ and $\{\tilde{\boldsymbol{e}}_{h_2} : ||\tilde{\boldsymbol{e}}_{h_2}||^2 \leq \epsilon_{h_2}^2\}$, where $\epsilon_{h_1}^2$ and $\epsilon_{h_2}^2$ are known constants that model the channel errors.

Then, our objective is to maximize the SNR of strong user while guaranteeing the correct signal decoding of the weak user for the channel mismatches, i.e., $\tilde{\boldsymbol{e}}_{h_1}$, $\tilde{\boldsymbol{e}}_{h_2}$, bounded in the known sets. Hence, the following robust beamforming design problem can be formulated:

$$\mathrm{P4}: \max_{\beta,\boldsymbol{w}_1,\boldsymbol{w}_2} \min_{\tilde{\boldsymbol{e}}_h \in \epsilon_h} \ (1-\beta)|\boldsymbol{h}_1^H\boldsymbol{w}_1|^2 \quad (35a)$$

$$s.t.\ \frac{(1-\beta)|\boldsymbol{h}_1^H\boldsymbol{w}_2|^2}{(1-\beta)|\boldsymbol{h}_1^H\boldsymbol{w}_1|^2 + 1} \geq \gamma, \quad (35b)$$

$$\frac{|\boldsymbol{h}_2^H\boldsymbol{w}_2|^2}{1+|\boldsymbol{h}_2^H\boldsymbol{w}_1|^2} + \zeta\beta|g|^2(|\boldsymbol{h}_1^H\boldsymbol{w}_1|^2 + |\boldsymbol{h}_1^H\boldsymbol{w}_2|^2) \geq \gamma, \quad (35c)$$

$$|\boldsymbol{h}_1^H\boldsymbol{w}_2|^2 \geq |\boldsymbol{h}_1^H\boldsymbol{w}_1|^2, \quad (35d)$$

$$|\boldsymbol{h}_2^H\boldsymbol{w}_2|^2 \geq |\boldsymbol{h}_2^H\boldsymbol{w}_1|^2, \quad (35e)$$

$$||\boldsymbol{w}_1||_2^2 + ||\boldsymbol{w}_2||_2^2 \leq P_{max}, \quad (35f)$$

$$0 \leq \beta \leq 1, \quad (35g)$$

where γ is the target SINR of user 2 and P_{max} is the maximum available power at the BS. It can be easily verified that problem P4 is nonconvex. This is not only due to the quadratic terms of the objective and constraints, but also for the hidden inner minimization constraint over $\tilde{\boldsymbol{e}}_h$.

Similarly, the first step is also to replace the beamforming vector $\boldsymbol{w}_i$ with semidefinite positive matrices $\boldsymbol{W}_i$, i.e,

$$\boldsymbol{W}_i = \boldsymbol{w}_i \boldsymbol{w}_i^H, \quad i = 1, 2. \tag{36}$$

Then, we decompose (35a) and (35b) by introducing several auxiliary variables to explore its hidden convexity. By denoting that $\boldsymbol{W} = \boldsymbol{W}_1 + \boldsymbol{W}_2$, the original problem P4 can be reformulated as

$$\begin{aligned}
\mathrm{P5}: \ & \max_{\beta, \boldsymbol{W}_1, \boldsymbol{W}_2} \min_{\tilde{\boldsymbol{e}}_h \in \epsilon_h} \ \mu && (37a)\\
& s.t. \ (\tilde{\boldsymbol{h}}_1 + \tilde{\boldsymbol{e}}_{h_1})^H \boldsymbol{W}_1 (\tilde{\boldsymbol{h}}_1 + \tilde{\boldsymbol{e}}_{h_1}) \geq \frac{\mu}{1-\beta}, && (37b)\\
& (\tilde{\boldsymbol{h}}_1 + \tilde{\boldsymbol{e}}_{h_1})^H \boldsymbol{W}_2 (\tilde{\boldsymbol{h}}_1 + \tilde{\boldsymbol{e}}_{h_1}) \geq \frac{\gamma(\mu+1)}{1-\beta}, && (37c)\\
& (\tilde{\boldsymbol{h}}_1 + \tilde{\boldsymbol{e}}_{h_1})^H \boldsymbol{W} (\tilde{\boldsymbol{h}}_1 + \tilde{\boldsymbol{e}}_{h_1}) \geq \frac{\gamma - t}{\zeta \beta |g|^2}, && (37d)\\
& \frac{(\tilde{\boldsymbol{h}}_2 + \tilde{\boldsymbol{e}}_{h_2})^H \boldsymbol{W}_2 (\tilde{\boldsymbol{h}}_2 + \tilde{\boldsymbol{e}}_{h_2})}{1 + (\tilde{\boldsymbol{h}}_2 + \tilde{\boldsymbol{e}}_{h_2})^H \boldsymbol{W}_1 (\tilde{\boldsymbol{h}}_2 + \tilde{\boldsymbol{e}}_{h_2})} \geq t, && (37e)\\
& (\tilde{\boldsymbol{h}}_1 + \tilde{\boldsymbol{e}}_{h_1})^H (\boldsymbol{W}_2 - \boldsymbol{W}_1) (\tilde{\boldsymbol{h}}_1 + \tilde{\boldsymbol{e}}_{h_1}) \geq 0, && (37f)\\
& (\tilde{\boldsymbol{h}}_2 + \tilde{\boldsymbol{e}}_{h_2})^H (\boldsymbol{W}_2 - \boldsymbol{W}_1) (\tilde{\boldsymbol{h}}_2 + \tilde{\boldsymbol{e}}_{h_2}) \geq 0, && (37g)\\
& \mathrm{Tr}(\boldsymbol{W}_1) + \mathrm{Tr}(\boldsymbol{W}_2) \leq P_{max}, && (37h)\\
& \boldsymbol{W}_1, \boldsymbol{W}_2 \succeq \boldsymbol{0} \ \text{ and } (35g), && (37i)
\end{aligned}$$

where μ and t are two auxiliary variables that can be respectively interpreted as the SNR of user 1 and $\mathrm{SINR}_2^{(1)}$. Note that problem P5 is a relaxed version by dropping the nonconvex rank-one constraints, i.e., $\mathrm{rank}(\boldsymbol{W}_\mathrm{i}) = 1, \ i = 1, 2$. The advantage of this relaxation lies in that the transformed inequalities are linear to $\boldsymbol{W}_1$ and $\boldsymbol{W}_2$. Although the rank-one constraints are dropped, we provide the following proposition to show that the relaxed problem P5 can still achieve an optimal solution which satisfies the rank-one constraints.

Proposition 2: There is always an optimal solution $(\boldsymbol{W}_1{}^*, \boldsymbol{W}_2{}^*)$ to problem P5 with $\mathrm{rank}(\boldsymbol{W}_\mathrm{i}^*) = 1, \ i = 1, 2$, whenever it is feasible.

Proof: The proof is provided in Appendix A.

Further, we note that in problem P5, only constraints (37b)-(37g) are nonconvex. To deal with the nonconvexity issues, we first transform the right-hand sides of (37b), (37c) and (37d) as follows:

$$\begin{aligned}
& \begin{bmatrix} \kappa_1 & \iota_1 \\ \iota_1 & 1-\beta \end{bmatrix} \succeq 0, && (38a)\\
& \iota_1^2 \geq \mu, && (38b)\\
& \begin{bmatrix} \kappa_2 & \iota_2 \\ \iota_2 & 1-\beta \end{bmatrix} \succeq 0, && (38c)\\
& \iota_2^2 \geq \gamma(\mu+1), && (38d)\\
& \begin{bmatrix} \kappa_3 & \iota_3 \\ \iota_3 & \zeta\beta|g|^2 \end{bmatrix} \succeq 0, && (38e)\\
& \iota_3^2 \geq \gamma - t, && (38f)
\end{aligned}$$

which consist of three LMIs (38a), (38c), and (38e), and three nonconvex quadratic inequalities (38b), (38d) and (38f) that need to be further transformed.

Then, the SCA method can be applied to iteratively approximate (38b), (38d) and (38f) by performing the first-order Taylor approximation as below

$$\begin{aligned}
& 2\iota_1^{(n)} \iota_1 - (\iota_1^{(n)})^2 \geq \mu, && (39a)\\
& 2\iota_2^{(n)} \iota_2 - (\iota_2^{(n)})^2 \geq \gamma(\mu+1), && (39b)\\
& 2\iota_3^{(n)} \iota_3 - (\iota_3^{(n)})^2 \geq \gamma - t, && (39c)
\end{aligned}$$

where $\iota_i^{(n)}, i = 1, 2, 3$, denotes the variable value of ι_i at the n-th iteration. As a result, the original nonconvex constraints can be approximated by SCA-based expressions and LMIs. The equivalence is guaranteed since (39a), (39b) and (39c) must hold with equality at optimum.

To deal with the inner minimization problem for the bounded error, (37b) can be first expressed as follows by introducing the inner bounded sets of channel mismatches:

$$\begin{aligned}
& \tilde{\boldsymbol{e}}_{h_1}^H \boldsymbol{W}_1 \tilde{\boldsymbol{e}}_{h_1} + 2Re(\tilde{\boldsymbol{h}}_1^H \boldsymbol{W}_1 \tilde{\boldsymbol{h}}_1) + \tilde{\boldsymbol{h}}_1^H \boldsymbol{W}_1 \tilde{\boldsymbol{e}}_1 - \kappa_1 \geq 0, && (40a)\\
& -\tilde{\boldsymbol{e}}_{h_1}^H \tilde{\boldsymbol{e}}_{h_1} + \epsilon_{h_1}^2 \geq 0. && (40b)
\end{aligned}$$

Then, in order to make the problem more tractable to solve, we introduce the *S*-procedure with the following lemma [33].

Lemma 2: Let $\boldsymbol{F}_1$, $\boldsymbol{F}_2$ be symmetric matrices, $\boldsymbol{g}_1$ and $\boldsymbol{g}_2$ be vectors, h_1 and h_2 be real numbers, then the following implication

$$\begin{aligned}
& \boldsymbol{x}^T \boldsymbol{F}_1 \boldsymbol{x} + 2\boldsymbol{x}^T g_1 \boldsymbol{x} + h_1 \leq 0, && (41a)\\
\Longrightarrow \ & \boldsymbol{x}^T \boldsymbol{F}_2 \boldsymbol{x} + 2\boldsymbol{x}^T g_2 \boldsymbol{x} + h_2 \leq 0, && (41b)
\end{aligned}$$

holds if and only if there exists a nonnegative number $\lambda \geq 0$ such that

$$\begin{bmatrix} \boldsymbol{F}_1 & \boldsymbol{g}_1 \\ \boldsymbol{g}_1^T & h_1 \end{bmatrix} \succeq \lambda \begin{bmatrix} \boldsymbol{F}_2 & \boldsymbol{g}_2 \\ \boldsymbol{g}_2^T & h_2 \end{bmatrix}, \tag{42}$$

provided that there exists a point $\hat{\boldsymbol{x}}$ with $\hat{\boldsymbol{x}}^T \boldsymbol{F}_1 \hat{\boldsymbol{x}} + 2\hat{\boldsymbol{x}}^T g_1 \boldsymbol{x} + h_1 \leq 0$.

According to Lemma 2, we note that both inequalities, i.e., (40a) and (40b), can be satisfied with a proper $\tilde{\boldsymbol{e}}_{h_1}$ if and only if there exists a $\nu_1 \geq 0$ such that

$$\begin{bmatrix} \nu_1 \boldsymbol{I}_{N_t} + \boldsymbol{W}_1 & \boldsymbol{W}_1 \tilde{\boldsymbol{h}}_1 \\ \tilde{\boldsymbol{h}}_1^H \boldsymbol{W}_1 & \tilde{\boldsymbol{h}}_1^H \boldsymbol{W}_1 \tilde{\boldsymbol{h}}_1 - \nu_1 \epsilon_{h_1}^2 - \kappa_1 \end{bmatrix} \succeq 0. \tag{43}$$

Notice that the inequality (43) is a convex LMI and can be easily implemented with standard convex solvers such as CVX [34]. Therefore, one can note that constraint (37b) has been transformed into convex forms.

After applying similar steps, (37c), (37d), (37f) and (37g) can be transformed into the following formulations:

$$\begin{bmatrix} \nu_2 \boldsymbol{I}_{N_t} + \boldsymbol{W}_2 & \boldsymbol{W}_2 \tilde{\boldsymbol{h}}_1 \\ \tilde{\boldsymbol{h}}_1^H \boldsymbol{W}_2 & \tilde{\boldsymbol{h}}_1^H \boldsymbol{W}_2 \tilde{\boldsymbol{h}}_1 - \nu_2 \epsilon_{h_1}^2 - \kappa_2 \end{bmatrix} \succeq 0, \tag{44a}$$

$$\begin{bmatrix} \nu_3 \boldsymbol{I}_{N_t} + \boldsymbol{W} & \boldsymbol{W} \tilde{\boldsymbol{h}}_1 \\ \tilde{\boldsymbol{h}}_1^H \boldsymbol{W} & \tilde{\boldsymbol{h}}_1^H \boldsymbol{W} \tilde{\boldsymbol{h}}_1 - \nu_3 \epsilon_{h_1}^2 - \kappa_3 \end{bmatrix} \succeq 0, \tag{44b}$$

$$\begin{bmatrix} \nu_4 \boldsymbol{I}_{N_t} + \boldsymbol{W}_2 - \boldsymbol{W}_1 & (\boldsymbol{W}_2 - \boldsymbol{W}_1) \tilde{\boldsymbol{h}}_1 \\ \tilde{\boldsymbol{h}}_1^H (\boldsymbol{W}_2 - \boldsymbol{W}_1) & \tilde{\boldsymbol{h}}_1^H (\boldsymbol{W}_2 - \boldsymbol{W}_1) \tilde{\boldsymbol{h}}_1 - \nu_4 \epsilon_{h_1}^2 \end{bmatrix} \succeq 0, \tag{44c}$$

Algorithm 2 SCA-Based Method to Solve P6

1: Given randomly generated feasible solution $\Lambda^{(0)}$.
2: n=0;
3: **Repeat**
4: Update $\Lambda^{(n)}$ by solving problem(49);
5: Set $n = n + 1$;
6: Until convergence or required number of iterations.

$$\begin{bmatrix} \nu_5 \boldsymbol{I}_{N_t} + \boldsymbol{W}_2 - \boldsymbol{W}_1 & (\boldsymbol{W}_2 - \boldsymbol{W}_1)\tilde{\boldsymbol{h}}_2 \\ \tilde{\boldsymbol{h}}_2^H (\boldsymbol{W}_2 - \boldsymbol{W}_1) & \tilde{\boldsymbol{h}}_2^H (\boldsymbol{W}_2 - \boldsymbol{W}_1)\tilde{\boldsymbol{h}}_2 - \nu_5 \epsilon_{h_1^2} \end{bmatrix} \succeq 0, \tag{44d}$$

where ν_2, ν_3, ν_4 and ν_5 are nonnegative variables and the above inequalities are all convex LMIs.

Now the only nonconvexity lies in the constraint (37e). To deal with it, we introduce some auxiliary variables and (37e) can be then written as

$$\left|\boldsymbol{h}_2^H \boldsymbol{w}_2\right|^2 \geq \kappa_4, \tag{45a}$$

$$\frac{\kappa_4 - t}{t} \geq \kappa_5, \tag{45b}$$

$$\left|\boldsymbol{h}_2^H \boldsymbol{w}_1\right|^2 \leq \kappa_5. \tag{45c}$$

For (45a) and (45c), *S*-procedure can be used to convert it into LMI formulation as follows

$$\begin{bmatrix} \nu_6 \boldsymbol{I}_{N_t} + \boldsymbol{W}_2 & \boldsymbol{W}_2 \tilde{\boldsymbol{h}}_2 \\ \tilde{\boldsymbol{h}}_2^H \boldsymbol{W}_2 & \tilde{\boldsymbol{h}}_2^H \boldsymbol{W} \tilde{\boldsymbol{h}}_2 - \nu_4 \epsilon_{h_2^2} - \kappa_4 \end{bmatrix} \succeq 0, \tag{46a}$$

$$\begin{bmatrix} \nu_7 \boldsymbol{I}_{N_t} - \boldsymbol{W}_1 & -\boldsymbol{W}_1 \tilde{\boldsymbol{h}}_2 \\ -\tilde{\boldsymbol{h}}_2^H \boldsymbol{W}_1 & -\tilde{\boldsymbol{h}}_2^H \boldsymbol{W}_1 \tilde{\boldsymbol{h}}_2 - \nu_5 \epsilon_{h_2^2} + \kappa_5 \end{bmatrix} \succeq 0. \tag{46b}$$

With respect to (45b), we apply the AGM inequality-based method to get its convex approximation that can be represented as:

$$(a^{(n)} \kappa_5)^2 + (t/(a^{(n)})^2 \leq 2\kappa_4 - 2t, \tag{47}$$

where $a^{(n)}$ represents the value of a at the n-th iteration and can be calculated as

$$a^{(n)} = \sqrt{\frac{t^{(n-1)}}{\kappa_5^{n-1}}}. \tag{48}$$

As a result, after applying the proposed approximation methods, the original problem P4 can be transformed into convex program. At the n-th iteration, the following optimization problem needs to be solved:

$$\text{P6}: \max_{\mu, t, \beta, \boldsymbol{w_1}, \boldsymbol{w_2}} \ \mu \tag{49a}$$

$$s.t.\ \nu_1, \nu_2, \nu_3, \nu_4, \nu_5, \nu_6, \nu_7 \geq 0, \tag{49b}$$

$$(38a),\ (38c),\ (38e),\ (39a),\ (39b), \tag{49c}$$

$$(39c),\ (43),\ (44a),\ (44b),\ (44c),\ (44d), \tag{49d}$$

$$(46a),\ (46b),\ (47),\ (37h) \text{ and } (37i). \tag{49e}$$

Accordingly, to solve the problem P6, the SCA-based iterative algorithm is outlined as Algorithm 2.

To prove that the above proposed algorithm converges, we provide the following propositions.

Proposition 3: A non-decreasing sequence of the objective values can be obtained from the proposed beamforming design in Algorithm 2, i.e., $\mu^{n+1} \geq \mu^n$. Thus, Algorithm 2 can continuously converge to a stationary point.

Proof: The proof is provided in Appendix B.

Though proposition 3 demonstrates that the proposed Algorithm 2 converges to a stationary point, the global optimality of the problem still cannot be guaranteed due to the nonconvex characteristic of problem P5. However, we can verify that the calculated solutions converge to a KKT point under some specific conditions, as summarized in the following proposition.

Proposition 4: The calculated solutions by using Algorithm 2 continuously converge to a KKT point of problem P5 when the iteration number tends to infinity.

Proof: The proof is provided in Appendix C.

V. Numerical Results

In this section, numerical results are provided to evaluate the performance of the proposed algorithms for a SWIPT-enabled robust cooperative NOMA system through Monte Carlo simulations. Firstly the outage-based constrained optimization problem will be examined, followed by the worst-case-based optimization problem. For both cases, we iteratively solve the robust optimization problems for 2,000 times. In the following simulations, it is assumed that the BS has two antennas, i.e. $N_t = 2$, while user 1 and user 2 each has one. The estimated channel coefficient can be modeled as $\tilde{\boldsymbol{h}}_k = \tilde{\boldsymbol{g}}_k d_k^{-\frac{\alpha}{2}}$, $k = \{1, 2\}$, where d_k is the distance from the BS to the k-th user, α is the path loss exponent. Here, we assume $\alpha = 2.5$ and $\tilde{\boldsymbol{g}}_k$ follows Rayleigh fading distribution with zero mean and unit variance. We set the EH efficiency ζ=0.7, unless otherwise stated. Without loss of generality, the bandwidth is set to be 1MHz. All the background noise power is assumed to be 1 Watt, and the transmit power is defined in dB relative to the noise power. In addition, for the purpose of system performance comparison, robust noncooperative NOMA, non-robust cooperative NOMA, and robust TDMA schemes are introduced as follows, which will be then compared with the proposed model:

- For robust noncooperative NOMA scheme, the BS serves two users simultaneously by performing NOMA and there is no cooperative transmission between user 1 and user 2. In addition, the BS only has imperfect CSI of two users and robust beamforming design is applied.
- For the non-robust cooperative NOMA scheme, the beamforming vectors and PS ratio for the cooperative NOMA system with perfect CSI is first obtained by using the beamforming design algorithm proposed in [13]. Since we want to check the performance of the non-robust design in a system with channel uncertainties, hence after obtaining $\boldsymbol{W}_i$ and β, if the constraints of problem P4 are not satisfied, the achievable rate of user 1 is 0. Otherwise, the rate of user 1 is computed by introducing the channel mismatches.
- For robust TDMA scheme, the system operates with TDMA mode and the time resource is equally allocated

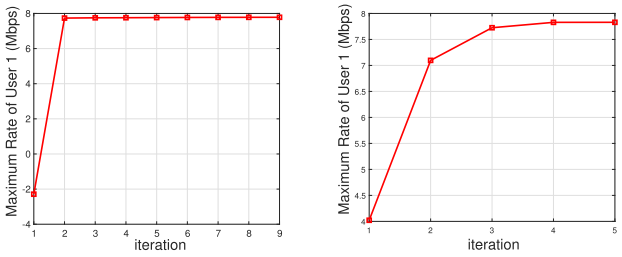

(a) For Algorithm 1 (b) For Algorithm 2

Fig. 2. The convergence procedure of two algorithms.

to two users. Furthermore, channel uncertainties exist in the connections between the BS and two users and robust design scheme is applied.

Before we examine the performance of the proposed SWIPT-enabled robust cooperative NOMA system, we first provide insight on the convergence property of the proposed algorithms. It can be observed from Fig. 2 that both algorithms converge to the maximum values within about 6 iterations, which proves the effectiveness of the proposed algorithms.

A. Outage-Based Constrained Optimization Simulation

In Fig. 3, the impact of the error variance is shown for the outage-based constrained optimization problem. Specifically, we set error covariances $\boldsymbol{C}_1$ and $\boldsymbol{C}_2$ be the same value as ϵ_h^2, the desired data rate of user 2 as 1 Mbps, the available maximum power at the BS be 20dB, and the outage is set to be 0.1 which means that the system has a chance of 90% or higher probability to satisfy the SINR requirements. The figure illustrates that the proposed SCA-based Algorithm 1 achieves similar system performance as exhaustive search method, but has significantly reduced computational complexity. Furthermore, we can observe that although the maximum achievable data rate of user 1 decreases for all of the schemes when the error variance becomes larger, the benefit of using the proposed SWIPT-enabled robust cooperative NOMA scheme becomes more significant since the gap between the proposed model and the other two schemes becomes larger. Moreover, it can be seen that the two NOMA schemes illustrated in this figure yield better performance than TDMA which shows the advantage of applying NOMA in the outage-based constrained optimization problem.

To investigate the performance of the proposed system model, Fig. 4 illustrates the maximum achievable data rate of user 1 versus the available transmission power at the BS for the following schemes: the proposed robust cooperative NOMA, cooperative NOMA with perfect CSI, robust noncooperative NOMA, noncooperative NOMA with perfect CSI, classical robust TDMA and TDMA with perfect CSI. This figure is plotted for the outage-based constrained optimization problem. To provide fair comparison results, we set ζ=1 here. First, it demonstrates that when perfect CSI is available at the BS, cooperative NOMA outperforms noncooperative NOMA in the low power region and achieves the same data rate in the high power regime. Moreover, Fig. 4 indicates that the proposed robust cooperative NOMA system always achieves better performance than the robust noncooperative NOMA

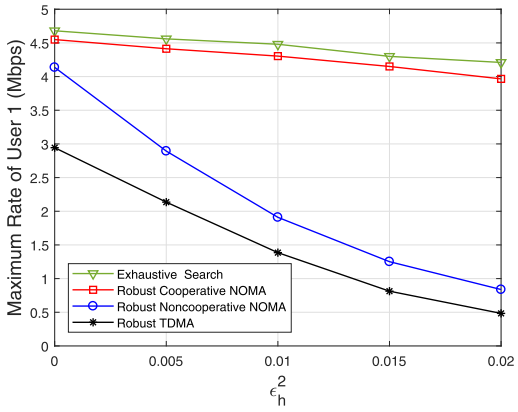

Fig. 3. Achievable rate of user 1 versus error variance with $\gamma = 1$, for the outage-based constrained optimization.

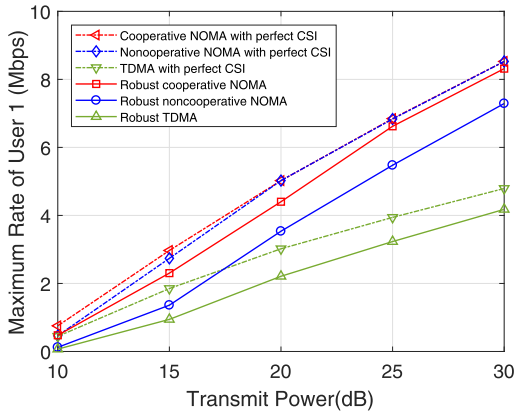

Fig. 4. Achievable rate of user 1 versus transmit power with $\gamma = 1$, for the outage-based constrained optimization.

and TDMA, which means that it is beneficial to adopt the cooperative transmission design for the situations with only imperfect CSI available.

Furthermore, in order to study the relationship between the achievable rate of user 1 and the target rate of user 2, we plot Fig. 5 to investigate the rate tradeoff between the two users for robust cooperative NOMA, robust noncooperative NOMA and robust TDMA schemes. This figure is plotted for the outage-based constrained optimization problem. Firstly, we can find that the robust cooperative NOMA yields the largest achievable data rate for user 1 among all three schemes. For example, when the target data rate of user 2 is 1.5 Mbps, the maximum achievable rate of user 1 for robust cooperative NOMA is 3.4 Mbps, while for the robust noncooperative NOMA and TDMA schemes, the maximum achievable rate of user 1 are 1.6 Mbps and 0.4 Mbps respectively. Furthermore, from Fig. 5, we can also notice that when the target data rate of user 2 increases, the achievable data rate of user 1 decreases for all three schemes as more power is allocated to user 2 in order to satisfy its rate requirements.

B. Worst-Case-Based Optimization Simulation

In Fig. 6, the impact of the channel mismatch for the worst-case-based optimization problem is presented. Here the desired QoS rate of user 2 is set to be 1 Mbps, and the

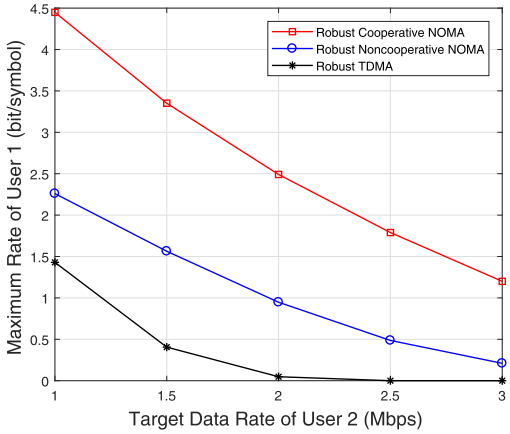

Fig. 5. Rates tradeoff for the outage-based constrained optimization with $\epsilon_h^2 = 0.01$ and $P_{max} = 20$dB.

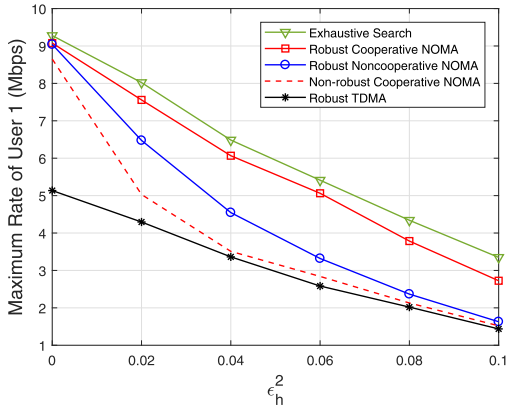

Fig. 6. Achievable rate of user 1 versus error variance with $\gamma = 1$ for the worst-case optimization.

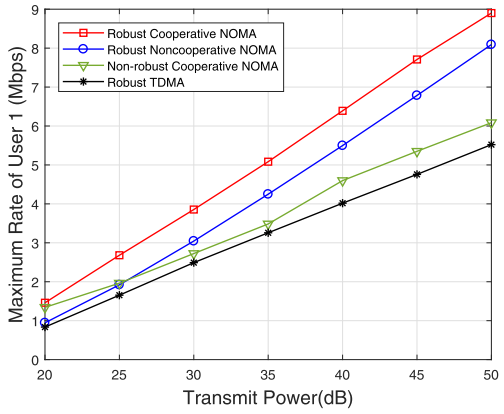

Fig. 7. Achievable rate of user 1 versus power with $\gamma = 1$ for the worst-case optimization.

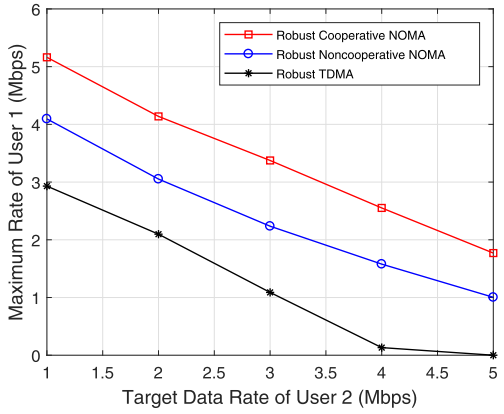

Fig. 8. Rates tradeoff for the worst-case optimization with $\epsilon_h^2 = 0.05$ and $P_{max} = 35dB$.

maximum available power is 35dB. Further, we set $\epsilon_{h_1}^2$ and $\epsilon_{h_2}^2$ to be the same value, denoted as ϵ_h^2. Similar to Fig. 3, Fig. 6 also shows that for the worst-case-based optimization problem, the performance of the proposed SCA-based robust cooperative design is close to that of the exhaustive search method. Furthermore, when perfect CSI is available, i.e., $\epsilon_h^2 = 0$, user 1 achieves almost the same rate for the proposed robust cooperative NOMA, non-robust cooperative NOMA and robust noncooperative NOMA. However, when there exists channel mismatch, the proposed robust cooperative scheme is more beneficial than the non-robust design. In addition, Fig. 6 shows that the robust cooperative NOMA always outperforms the robust noncooperative NOMA scheme. The reason is that, for the robust cooperative scheme, the cooperative phase with perfect CSI can be utilized to improve the weak user's reception reliability under the condition of limited available power at the BS. Furthermore, though the gap between the robust noncooperative NOMA and robust TDMA scheme decreases with the error variance, it can still be observed that NOMA scheme always performs better than TDMA scheme which demonstrates the superiority of NOMA. Specifically, the advantage of NOMA is more significant when the error variance ϵ_h^2 is relatively small.

To study the performance of the proposed robust cooperative NOMA scheme, Fig. 7 is plotted to compare different schemes: robust cooperative NOMA, robust noncooperative NOMA, non-robust cooperative NOMA and traditional robust TDMA, for the worst-case optimization. The channel mismatch is set as $\epsilon_{h_1}^2 = \epsilon_{h_2}^2 = 0.05$. Firstly, we can notice that the proposed SWIPT-enabled robust cooperative NOMA produces the best performance among all schemes. Especially, the robust design improves the data rate of user 1 greatly, compared to its non-robust counterparts. Furthermore, both the proposed scheme and the robust noncooperative NOMA outperforms the traditional robust TDMA scheme which indicates the advantage of NOMA in improving system spectral efficiency when channel uncertainty exists.

Fig. 8 shows the influence of user 2's target data rate on the achievable data rate performance of user 1 for the robust cooperative NOMA, robust noncooperative NOMA and robust TDMA schemes. This figure is illustrated based on the worst-case optimization. Firstly, Fig. 8 demonstrates that the proposed SWIPT-enabled robust cooperative NOMA achieves higher maximum achievable rate for user 1, compared to the robust noncooperative NOMA and TDMA schemes. In addition, Fig. 8 shows that the achievable data rate of user 1 decreases with the increase of target data rate of

user 2 for all schemes. This is because when user 2 has a higher target data rate, more power is allocated to satisfy its requirement and as a result, the power available to user 1 becomes less.

VI. Conclusion

In this paper, we have investigated the robust beamforming and PS design to maximize the strong user's data rate for a SWIPT-enabled robust cooperative NOMA system. Two kinds of channel uncertainties are considered, which respectively lead to an outage-based SINR constrained optimization and a worst-case-based optimization problem. For both cases, the original problem was first transformed into a more tractable form by using SDR technique. Specifically, as to the outage-based SINR constrained optimization problem, the Bernstein-type inequality was applied to convert the probabilistic constraints into manageable and computable approximations that can be globally solved by two-dimensional exhaustive search. An iterative method was further developed to reduce the high complexity. On the other hand, to solve the worst-case-based optimization problem, the rank-one optimality of the SDR approach was first proved. Then, by applying the *S*-procedure, the nonconvex problem was reformulated as convex ones which can be finally solved using the proposed SCA-based algorithm. Simulation results demonstrated the superiority of the proposed SWIPT-enabled cooperation in robust NOMA design over other schemes.

Appendix A
Proof of Proposition 2

For any given β and t, problem P5 can be degraded into the following problem:

$$\mathrm{P7}: \max_{\beta,\boldsymbol{W}_1,\boldsymbol{W}_2} \min_{\tilde{\boldsymbol{e}}_h\in\epsilon_h} \ \mu \tag{50a}$$

$$s.t.\ (\tilde{\boldsymbol{h}}_1+\tilde{\boldsymbol{e}}_{h_1})^H\boldsymbol{W}_1(\tilde{\boldsymbol{h}}_1+\tilde{\boldsymbol{e}}_{h_1}) \geq \frac{\mu}{1-\beta}, \tag{50b}$$

$$(\tilde{\boldsymbol{h}}_1+\tilde{\boldsymbol{e}}_{h_1})^H\boldsymbol{W}_2(\tilde{\boldsymbol{h}}_1+\tilde{\boldsymbol{e}}_{h_1}) \geq \frac{\gamma(\mu+1)}{1-\beta}, \tag{50c}$$

$$\frac{\mu}{1-\beta}+\frac{\gamma(\mu+1)}{1-\beta} \leq \frac{\gamma-t}{\zeta\beta|g|^2}, \tag{50d}$$

$$(\tilde{\boldsymbol{h}}_2+\tilde{\boldsymbol{e}}_{h_2})^H(\boldsymbol{W}_2-t\boldsymbol{W}_1)(\tilde{\boldsymbol{h}}_2+\tilde{\boldsymbol{e}}_{h_2}) \geq \max\{t,\frac{1}{2}\}, \tag{50e}$$

$$\gamma(\mu+1) \geq \mu, \tag{50f}$$

$$\mathrm{Tr}(\boldsymbol{W}_1)+\mathrm{Tr}(\boldsymbol{W}_2) \leq P_{max}, \tag{50g}$$

$$\boldsymbol{W}_1,\boldsymbol{W}_2 \succeq \boldsymbol{0}. \tag{50h}$$

Particularly, (50d) is acquired by substituting the constraints of (37b) and (37c) into (37d) and the inequality can be satisfied based on the fact that the summation of two individual lower bound values is always smaller or equal to the global lower bound. Constraint (50f) is obtained by replacing constraint (37f) with (37b) and (37c), and (50e) is listed to assure that both constraints, i.e., (37e) and (37g), are satisfied. Assume that P7 is feasible and it is also dual feasible. As can be seen from problem P7, there are four linear constraints (50b, 50c, 50e and 50g) related to the optimal solution $(\boldsymbol{W}_1{}^*, \boldsymbol{W}_2{}^*)$ and according to [35, Th. 3.2], we have that

$$\mathrm{rank}^2(\boldsymbol{W}_1{}^*)+\mathrm{rank}^2(\boldsymbol{W}_2{}^*) \leq 4. \tag{51}$$

If P7 is feasible, from (50b), we can find that $\boldsymbol{W}_1{}^* \succeq \boldsymbol{0}$ and $\boldsymbol{W}_1{}^* \neq \boldsymbol{0}$; from (50c), we have that $\boldsymbol{W}_2{}^* \succeq \boldsymbol{0}$ and $\boldsymbol{W}_2{}^* \neq \boldsymbol{0}$. Further, with constraint (51) considered, we can conclude that only when $\mathrm{rank}(\boldsymbol{W}_{\mathrm{i}}^*)=1, i=1,2$, the inequality (51) can be satisfied. Hence, we can conclude that problem P4 always has an optimal solution $\boldsymbol{W}_1{}^*$ and $\boldsymbol{W}_2{}^*$. Then, the optimal beamforming vector $\boldsymbol{w}_1{}^*$ and $\boldsymbol{w}_2{}^*$ can be respectively obtained from $\boldsymbol{W}_1{}^*$ and $\boldsymbol{W}_2{}^*$ by using eigen-decomposition. Otherwise, a suboptimal solution can be attained by Gaussian randomization. The proof is completed.

Appendix B
Proof of Proposition 3

In order to prove that the acquired objective value is non-decreasing for each iteration, we need to first demonstrate that the solution to problem P6 at the n-th iteration is also a feasible point for the iteration $(n+1)$.

Let us assume that the optimal solutions to problem P6 at the n-th iteration are $\boldsymbol{W}_1^*$, $\boldsymbol{W}_2^*$, ι_1^*, ι_2^*, ι_3^*, and a^*. The constraints which use the SCA-based method to get convex approximation are constraints (39a), (39b) and (39c). Here, we take the constraint (39a) as an example.

$$2\iota_1^{(n)}\iota_1^*-(\iota_1^{(n)})^2 \geq \mu. \tag{52}$$

We then replace the variables at the iteration (n+1) with the optimal solutions obtained in iteration n, e.g., $\iota_1^{(n+1)}=\iota_1^*$. It is obvious that the constraints (39a) and (43) can be satisfied. In addition, during the iteration of $(n+1)$ for (38a) with the updated parameter, the following result can be obtained:

$$2\iota_1^*\iota_1^*-(\iota_1^*)^2 = \iota_1^{*2} \tag{53a}$$

$$\geq 2\iota_1^{(n)}\iota_1^*-(\iota_1^{(n)})^2 \tag{53b}$$

$$\geq \mu, \tag{53c}$$

where (53a) is derived by substituting the solutions of iteration n. The inequality (53b) is gained by performing the first-order Taylor approximation for ι_1^{*2} around ι_1^* which is a lower bound of the original function. Finally, we can get (53c) with the application of (52). Similarly, the optimal solutions obtained at the n-th iteration also satisfy the constraints (39b) and (39c) for the iteration $n+1$. The detailed analysis for the constraints (39b) and (39c) at iteration $(n+1)$ is omitted here, but can be provided following similar steps.

In conclusion, it can be proved that the optimal solution of the n-th iteration obtained from Algorithm 2 is a feasible point for problem P6 at the $(n+1)$-th iteration. As problem P6 is a concave problem, the objective value at the $(n+1)$-th iteration is larger or equal to that achieved from the n-th iteration. Hence, the proof is completed and the proposition is proved.

APPENDIX C
PROOF OF PROPOSITION 4

Let $\Lambda^n = \{\boldsymbol{W}_1^n, \boldsymbol{W}_2^n, \iota_1^n, \iota_2^n, \iota_3^n, a^n\}$ be the solution derived from Algorithm 2 during the n-th iteration. According to proposition 3, we have that $\Lambda^n \rightarrow \Lambda^*$ as $n \rightarrow \infty$ where Λ^* represents the optimal solution to P6. Besides, with the application of the SCA method, the introduced lower bound of (39a) has the same value and gradient value around the point Λ^n for any iterations (which still holds as $n \rightarrow \infty$). Therefore, we can conclude that Algorithm 2 can continuously coverage to a KKT point of problem P5 when the iteration number tends to infinity based on the above property.

REFERENCES

[1] J. G. Andrews *et al.*, "What will 5G be?" *IEEE J. Sel. Areas Commun.*, vol. 32, no. 6, pp. 1065–1082, Jun. 2014.

[2] L. Lv, J. Chen, and Q. Ni, "Cooperative non-orthogonal multiple access in cognitive radio," *IEEE Commun. Lett.*, vol. 20, no. 10, pp. 2059–2062, Oct. 2016.

[3] B. Su, Q. Ni, W. Yu, and H. Pervaiz, "Outage constrained robust beamforming design for SWIPT-enabled cooperative NOMA system," in *Proc. IEEE Int. Conf. Commun. (ICC)*, May 2019.

[4] J. Ye *et al.*, "Cooperative communications with wireless energy harvesting over Nakagami-m fading channels," *IEEE Trans. Commun.*, vol. 65, no. 12, pp. 5149–5164, Dec. 2017.

[5] W. Yu, L. Musavian, and Q. Ni, "Link-layer capacity of NOMA under statistical delay QoS guarantees," *IEEE Trans. Commun.*, vol. 66, no. 10, pp. 4907–4922, Oct. 2018.

[6] Z. Ding, M. Peng, and H. V. Poor, "Cooperative non-orthogonal multiple access in 5G systems," *IEEE Commun. Lett.*, vol. 19, no. 8, pp. 1462–1465, Aug. 2015.

[7] W. Yu, L. Musavian, and Q. Ni, "Tradeoff analysis and joint optimization of link-layer energy efficiency and effective capacity toward green communications," *IEEE Trans. Wireless Commun.*, vol. 15, no. 5, pp. 3339–3353, May 2016.

[8] R. Zhang and C. K. Ho, "MIMO broadcasting for simultaneous wireless information and power transfer," *IEEE Trans. Wireless Commun.*, vol. 12, no. 5, pp. 1989–2001, May 2013.

[9] G. Pan, H. Lei, Y. Yuan, and Z. Ding, "Performance analysis and optimization for SWIPT wireless sensor networks," *IEEE Trans. Commun.*, vol. 65, no. 5, pp. 2291–2302, May 2017.

[10] J. Gong and X. Chen, "Achievable rate region of non-orthogonal multiple access systems with wireless powered decoder," *IEEE J. Sel. Areas Commun.*, vol. 35, no. 12, pp. 2846–2859, Dec. 2017.

[11] M. Hedayati and I.-M. Kim, "On the performance of OMA and NOMA in the Two-user SWIPT system," *IEEE Trans. Veh. Technol.*, vol. 67, no. 11, pp. 11258–11263, Nov. 2018.

[12] Y. Liu, Z. Ding, M. Elkashlan, and H. V. Poor, "Cooperative non-orthogonal multiple access with simultaneous wireless information and power transfer," *IEEE J. Sel. Areas Commun.*, vol. 34, no. 4, pp. 938–953, Apr. 2016.

[13] Y. Xu *et al.*, "Joint beamforming and power-splitting control in downlink cooperative SWIPT NOMA systems," *IEEE Trans. Signal Process.*, vol. 65, no. 18, pp. 4874–4886, Sep. 2017.

[14] C. C. Zarakovitis, Q. Ni, and J. Spiliotis, "Energy-efficient green wireless communication systems with imperfect CSI and data outage," *IEEE J. Sel. Areas Commun.*, vol. 34, no. 12, pp. 3108–3126, Dec. 2016.

[15] C. C. Zarakovitis, Q. Ni, D. E. Skordoulis, and M. G. Hadjinicolaou, "Power-efficient cross-layer design for OFDMA systems with heterogeneous QoS, imperfect CSI, and outage considerations," *IEEE Trans. Veh. Technol.*, vol. 61, no. 2, pp. 781–798, Feb. 2012.

[16] Q. Zhang, Q. Li, and J. Qin, "Robust beamforming for nonorthogonal multiple-access systems in MISO channels," *IEEE Trans. Veh. Technol.*, vol. 65, no. 12, pp. 10231–10236, Dec. 2016.

[17] F. Alavi, K. Cumanan, Z. Ding, and A. G. Burr, "Robust beamforming techniques for non-orthogonal multiple access systems with bounded channel uncertainties," *IEEE Commun. Lett.*, vol. 21, no. 9, pp. 2033–2036, Sep. 2017.

[18] S. Chinnadurai, P. Selvaprabhu, Y. Jeong, X. Jiang, and M. H. Lee, "Worst-case energy efficiency maximization in a 5G Massive MIMO-NOMA system," *Sensors*, vol. 17, no. 9, p. 2139, 2017.

[19] Y. Sun, D. W. K. Ng, J. Zhu, and R. Schober. (2017). "Robust and secure resource allocation for full-duplex MISO multicarrier NOMA systems." [Online]. Available: https://arxiv.org/abs/1710.01391

[20] E. Hossain and M. Hasan, "5G cellular: Key enabling technologies and research challenges," *IEEE Instrum. Meas. Mag.*, vol. 18, no. 3, pp. 11–21, Jun. 2015.

[21] Z. Zhu, Z. Chu, Z. Wang, and I. Lee, "Outage constrained robust beamforming for secure broadcasting systems with energy harvesting," *IEEE Trans. Wireless Commun.*, vol. 15, no. 11, pp. 7610–7620, Nov. 2016.

[22] Z. Chu, H. Xing, M. Johnston, and S. L. Goff, "Secrecy rate optimizations for a MISO secrecy channel with multiple multiantenna eavesdroppers," *IEEE Trans. Wireless Commun.*, vol. 15, no. 1, pp. 283–297, Jan. 2016.

[23] Y. Hao, Q. Ni, H. Li, and S. Hou, "Robust multi-objective optimization for EE-SE tradeoff in D2D communications underlaying heterogeneous networks," *IEEE Trans. Commun.*, vol. 66, no. 10, pp. 4936–4949, Oct. 2018.

[24] A. W. C. Lim and V. K. N. Lau, "On the fundamental tradeoff of spatial diversity and spatial multiplexing of MISO/SIMO links with imperfect CSIT," *IEEE Trans. Wireless Commun.*, vol. 7, no. 1, pp. 110–117, Jan. 2008.

[25] Z. Ding *et al.*, "Impact of user pairing on 5G nonorthogonal multiple-access downlink transmissions," *IEEE Trans. Veh. Technol.*, vol. 65, no. 8, pp. 6010–6023, Aug. 2016.

[26] L. Liu, R. Zhang, and K.-C. Chua, "Multi-antenna wireless powered communication with energy beamforming," *IEEE Trans. Commun.*, vol. 62, no. 12, pp. 4349–4361, Dec. 2014.

[27] M. F. Hanif, Z. Ding, T. Ratnarajah, and G. K. Karagiannidis, "A minorization-maximization method for optimizing sum rate in the downlink of non-orthogonal multiple access systems," *IEEE Trans. Signal Process.*, vol. 64, no. 1, pp. 76–88, Jan. 2016.

[28] Q. Shi, L. Liu, W. Xu, and R. Zhang, "Joint transmit beamforming and receive power splitting for MISO SWIPT systems," *IEEE Trans. Wireless Commun.*, vol. 13, no. 6, pp. 3269–3280, Jun. 2014.

[29] S. Mallick, M. M. Rashid, and V. K. Bhargava, "Joint relay selection and power allocation for decode-and-forward cellular relay network with channel uncertainty," *IEEE Trans. Wireless Commun.*, vol. 11, no. 10, pp. 3496–3508, Oct. 2012.

[30] M. B. Shenouda and T. N. Davidson, "Probabilistically-constrained approaches to the design of the multiple antenna downlink," in *Proc. 42nd IEEE Asilomar Conf. (SSC)*, Oct. 2008, pp. 1120–1124.

[31] I. Bechar. (2009). "A Bernstein-type inequality for stochastic processes of quadratic forms of Gaussian variables." [Online]. Available: https://arxiv.org/abs/0909.3595

[32] M. K. Vamanamurthy and M. Vuorinen, "Inequalities for means," *J. Math. Anal. Appl.*, vol. 183, no. 1, pp. 155–166, 1994.

[33] S. Boyd and L. Vandenberghe, *Convex Optimization*. Cambridge, U.K.: Cambridge Univ. Press, 2004.

[34] M. Grant, S. Boyd, and Y. Ye, *CVX: MATLAB Software for Disciplined Convex Programming*. Cambridge, U.K.: Cambridge Univ. Press, 2008.

[35] Y. Huang and D. P. Palomar, "Rank-constrained separable semidefinite programming with applications to optimal beamforming," *IEEE Trans. Signal Process.*, vol. 58, no. 2, pp. 664–678, Feb. 2010.

Authors' photographs and biographies not available at the time of publication.